

Tuning of the spin-orbit interaction in a quantum dot by an in-plane magnetic fieldM. P. Nowak,^{1,2} B. Szafran,¹ F. M. Peeters,² B. Partoens,² and W. J. Pasek¹¹*Faculty of Physics and Applied Computer Science, AGH University of Science and Technology, al. Mickiewicza 30, PL-30-059 Kraków, Poland*²*Departement Fysica, Universiteit Antwerpen, Groenenborgerlaan 171, BE-2020 Antwerpen, Belgium*

(Received 7 February 2011; revised manuscript received 28 April 2011; published 30 June 2011)

Using an exact-diagonalization approach we show that one- and two-electron InAs quantum dots exhibit an avoided crossing in the energy spectra that is induced by the spin-orbit coupling in the presence of an in-plane external magnetic field. The width of the avoided crossings depends strongly on the orientation of the magnetic field, which reveals the intrinsic anisotropy of the spin-orbit-coupling interactions. We find that for specific orientations of the magnetic field avoided crossings vanish. A value of this orientation can be used to extract the ratio of the strength of Rashba and Dresselhaus interactions. The spin-orbit anisotropy effects for various geometries and orientations of the confinement potential are discussed. Our analysis explains the physics behind the recent measurements performed on a gated self-assembled quantum dot [S. Takahashi *et al.*, *Phys. Rev. Lett.* **104**, 246801 (2010)].

DOI: 10.1103/PhysRevB.83.245324

PACS number(s): 73.21.La

I. INTRODUCTION

Over the past decade there has been a growing interest in the study of the spin-orbit (SO) interaction in semiconductor low-dimensional systems motivated by the possibility of coherent spin manipulation.^{1–13} The Hamiltonians describing the SO coupling resulting from the inversion asymmetry of the material (Dresselhaus¹⁴ coupling) or the specific structure of the device (Rashba¹⁵ interaction) are not invariant with respect to the rotation of the spin or the momentum operators separately, and, consequently, spin-orbit-coupled systems possess intrinsic anisotropic properties. This anisotropy has been thoroughly studied for delocalized systems.^{4,5} In particular, in transport experiments, the dependence of the conductance of a narrow quantum wire on the direction of the external magnetic field can be used to determine the reciprocal strengths of the Rashba and Dresselhaus couplings.⁶ The anisotropy of the spin-orbit interaction is translated into an anisotropic effective magnetic field⁷ for a moving electron modifying the electron spin state. This effective magnetic field can be used to perform rotations of spin and thus to construct quantum gates⁸ or a spin-field effect transistor.^{9,10} Moreover, the spin-orbit coupling is responsible for anisotropic corrections¹¹ to the spin swap in a two-qubit quantum gate¹² because it results in the precession of spin-packets tunneling between the two quantum dots.¹³

For electrons localized in a quantum dot, the SO coupling results in avoided crossings (AC) in the energy spectra¹⁶ and spin relaxation¹⁷ mediated by phonons with a relaxation rate dependent on the orientation of the external magnetic field.¹⁸ The energetic effects of the SO interaction are usually weak. Only recently SO-induced AC were experimentally measured on quantum dots that were situated in gated nanowires^{19,20} and gated self-assembled quantum dots.²¹ The latter experiment studied changes of the width of AC for different orientations of the magnetic field, which extended the previous studies that were focused on a comparison of the spin-splittings for vertical and in-plane alignment of a magnetic field^{22,23} in circularly symmetric confinement potentials.

In the present work, we explain the physics underlying the observations of Ref. 21. To the best of our knowledge, the present paper explains for the first time the oscillatory dependence of the width of AC on the direction of the in-plane magnetic field. The latter turns out to be the consequence of the influence of the individual SO couplings and the anisotropy of the confinement potential. This conclusion is supported by an exact three-dimensional calculation of the energy spectra of one- and two-electron spin-orbit-coupled quantum dots.

We show that for quantum dots with a confinement potential elongated in [100] direction for pure Rashba (or pure Dresselhaus) coupling, the AC disappears when the magnetic field is aligned along the short (or long) axis of the dot. We show how this can be understood from the form of the SO Hamiltonians and the approximate parity of the one-electron wave functions. The dependence of the AC width on the direction of the magnetic field turns to be a $|\sin\phi|$ -shaped function, and when both couplings are present, this function is shifted by an amount that depends on the relative strength of both interactions. This shift is affected by the orientation of the dot within the [001] plane due to the SO bulk-induced anisotropy (Dresselhaus term). For completeness, we also study the influence of the dot shape. We show that for a square-based quantum dot the anisotropic dependence of the AC width is only observed when both couplings are present.²³ Moreover, we show that for increased height of the dot, the orbital effect of the magnetic field modifies the energy spectrum, but the shape of the dependence of the anticrossing width on the direction of the in-plane magnetic field remains unaltered.

The present work is organized as follows: we start with an outline of our theoretical approach in Sec. II. In Sec. III, we present our numerical results starting from the single-electron case, which provides us with a physical insight of the reasons for the SO-coupling anisotropy. We continue by studying different orientations and geometries of the dot, and we end the section with the two-electron case that allows for a direct comparison with the recent experimental data of Ref. 21. We end with a concluding discussion in Sec. IV and a summary in Sec. V.

II. THEORY

A. Model

Our aim is to calculate the energy spectra of one and two electrons confined in a three-dimensional quantum dot in the presence of SO coupling and a magnetic field oriented within the quantum-dot plane. The effect of the spin-orbit coupling on the energy is very small, requiring a very high numerical precision when evaluating the energy spectrum. We assume that the quantum dot is cuboid in shape and that the confinement potential is separable, namely, $V(\mathbf{r}) = V_x(x) + V_y(y) + V_z(z)$. Moreover, we assume that the one-dimensional confinement potentials V_x , V_y , and V_z can be described by an infinite quantum-well model. This is a reasonable approximation for not too small quantum dots. Under these assumptions one can construct a sufficiently precise solver for the two-electron problem. We consider a quantum dot with a varied in-plane orientation with respect to the crystal host. The z axis is taken along the [001] crystal direction, which is also the vertical axis of the dot. The orientation of the dot is described by a rotation of the x and y directions (which are the axes of the dot) with respect to the [100] and [010] crystal directions. The outline of our quantum dot and the coordinate system used is depicted in Fig. 1.

B. Method

We employ the effective mass approximation with a single-electron Hamiltonian of the form

$$h = \left[\frac{\hbar^2 \mathbf{k}^2}{2m^*} + V(\mathbf{r}) \right] \mathbf{1} + \frac{1}{2} g \mu_B \mathbf{B} \sigma + H_{\text{BIA}} + H_{\text{SIA}}, \quad (1)$$

where $\mathbf{k} = -i\nabla + e\mathbf{A}/\hbar$, $\mathbf{1}$ is the identity matrix, $V(\mathbf{r})$ defines the confining potential, and H_{BIA} and H_{SIA} are the spin-orbit-coupling Hamiltonians. The x , y , and z directions are taken

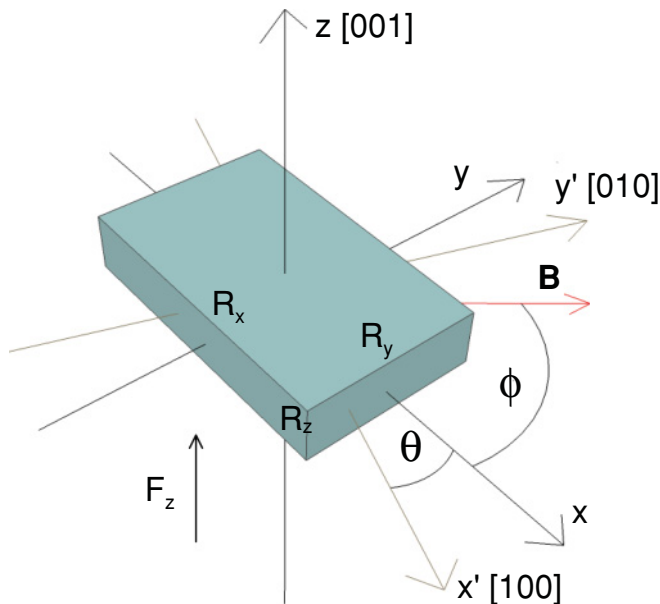


FIG. 1. (Color online) Schematics of the quantum dot system with the used coordinate system fixed to the quantum dot. The crystallographic directions of the InAs host lattice are also indicated together with the direction of the in-plane magnetic field.

along the axes of the dot. But notice that the SO-interaction Hamiltonians are defined in a coordinate system with axes parallel to the [100], [010], and [001], which we denote with x' , y' , and z . Both coordinate systems are transformed into each other by an in-plane rotation by an angle θ .

We introduce the Rashba coupling with Hamiltonian,

$$H_{\text{SIA}} = \alpha \nabla' V \cdot (\sigma' \times \mathbf{k}'), \quad (2)$$

where α defines the coupling strength. For infinite-quantum-well confinement the term $\nabla' V$ within the dot is equal to the external electric field. We neglect the influence of the in-plane component of the electric field²⁴ and obtain the Rashba Hamiltonian in the form

$$H_{\text{SIA}} = \alpha \frac{\partial V}{\partial z} (\sigma_{x'} k_{y'} - \sigma_{y'} k_{x'}). \quad (3)$$

Thus the electric field is in the z direction, which is incorporated by taking a nonzero slope of the bottom of $V_z(z)$.

Inversion asymmetry of the crystal lattice results in a Dresselhaus SO coupling that is described by the Hamiltonian

$$H_{\text{BIA}} = \gamma [\sigma_{x'} k_{x'} (k_z^2 - k_{y'}^2) + \sigma_{y'} k_{y'} (k_{x'}^2 - k_z^2) + \sigma_z k_z (k_{y'}^2 - k_{x'}^2)], \quad (4)$$

where γ is the coupling constant.

The coordinate system used for the SO coupling can be transformed into the coordinate system used for the quantum dot through the transformation:

$$\begin{aligned} x' &= x \cos \theta - y \sin \theta, \\ y' &= x \sin \theta + y \cos \theta, \end{aligned} \quad (5)$$

which applies both to the Pauli matrices σ and the coordinates of the momentum operator.

We include an in-plane magnetic field of orientation $\mathbf{B} = B(\cos \phi, \sin \phi, 0)$, which is described by the gauge $\mathbf{A} = B(z \sin \phi, 0, y \cos \phi)$. The magnetic field vector, \mathbf{B} , for $\phi = 0$ is oriented along the x direction (see Fig. 1).

The one-electron Hamiltonian, Eq. (1), can be rewritten in the form $h = h_x + h_y + h_z + h_{\text{ns}}$, where

$$h_x = -\frac{\hbar^2}{2m^*} \frac{\partial^2}{\partial x^2} + V_x(x), \quad (6)$$

$$h_y = -\frac{\hbar^2}{2m^*} \frac{\partial^2}{\partial y^2} + V_y(y) + \frac{e^2 B^2}{2m^*} y^2 \cos^2 \phi, \quad (7)$$

$$h_z = -\frac{\hbar^2}{2m^*} \frac{\partial^2}{\partial z^2} + V_z(z) + \frac{e^2 B^2}{2m^*} z^2 \sin^2 \phi, \quad (8)$$

are spin-independent parts separable in the x , y , and z directions, and

$$\begin{aligned} h_{\text{ns}} &= -\frac{i\hbar e B}{m^*} \left(z \sin \phi \frac{\partial}{\partial x} + y \cos \phi \frac{\partial}{\partial z} \right) \\ &+ \frac{1}{2} g \mu_b B [\sigma_x \cos \phi + \sigma_y \sin \phi] + H_{\text{SIA}} + H_{\text{BIA}} \end{aligned} \quad (9)$$

is the nonseparable part that contains the spin-dependent terms.

The eigenenergies and the eigenvectors, $\psi_x(x)$, $\psi_y(y)$, and $\psi_z(z)$, of the Hamiltonians, h_x , h_y and h_z , are calculated

separately on an one-dimensional mesh of $N_{1D} = 1000$ points. In a next step, we diagonalize h_{ns} in a basis of products of the eigenstates, $\psi_x(x)$, $\psi_y(y)$, and $\psi_z(z)$, resulting in three-dimensional spin-orbitals $\psi(\mathbf{r}, \sigma)$. We typically take $N_x = N_y = 20$ and $N_z = 10$ one-dimensional eigenstates (we assumed $R_z \ll R_x, R_y$), which, including the degeneracy of the spin, gives a basis consisting of 8000 elements that results in an accuracy better than $5 \mu\text{eV}$.

We solve the two-electron problem as described by the Hamiltonian

$$H = h_1 + h_2 + \frac{e^2}{4\pi\epsilon\epsilon_0|\mathbf{r}_1 - \mathbf{r}_2|} \quad (10)$$

using the configuration-interaction approach. In our numerical calculation, we take the dielectric constant $\epsilon = 14.6$ for InAs. The Hamiltonian in Eq. (10) is diagonalized in a basis constructed of antisymmetrized single-electron spin-orbitals $\psi(\mathbf{r}, \sigma)$,

$$\Psi = \frac{1}{\sqrt{2}} \sum_{i=1}^n \sum_{j=i+1}^n [\psi_i(\mathbf{1})\psi_j(\mathbf{2}) - \psi_i(\mathbf{2})\psi_j(\mathbf{1})], \quad (11)$$

where $\mathbf{1}$ and $\mathbf{2}$ are the spatial (\mathbf{r}) and spin (σ) coordinates of the corresponding electron. The electron-electron interaction matrix element requires the calculation of integrals of the form

$$\begin{aligned} & \frac{e^2}{4\pi\epsilon_0} \langle \psi_i(\mathbf{r}_1)\psi_j(\mathbf{r}_2) | \frac{1}{\epsilon|\mathbf{r}_1 - \mathbf{r}_2|} | \psi_k(\mathbf{r}_1)\psi_l(\mathbf{r}_2) \rangle \\ &= e \int d^3\mathbf{r}_1 \psi_i^*(\mathbf{r}_1)\psi_k(\mathbf{r}_1) \int d^3\mathbf{r}_2 \frac{e}{4\pi\epsilon_0} \frac{\psi_j^*(\mathbf{r}_2)\psi_l(\mathbf{r}_2)}{\epsilon|\mathbf{r}_1 - \mathbf{r}_2|} \\ &= e \int d^3\mathbf{r}_1 \psi_i^*(\mathbf{r}_1)\psi_k(\mathbf{r}_1) V_{jl}(\mathbf{r}_1). \end{aligned} \quad (12)$$

A direct calculation of these six dimensional integrals requires an enormous numerical cost. Therefore, we use a method²⁵ in which the innermost integral is attributed to an electric potential, $V_{jl}(\mathbf{r}_1)$, originating from an electric charge distribution, $\psi_j^*(\mathbf{r}_2)\psi_l(\mathbf{r}_2)$. We calculate the electric potential by solving the Poisson equation $\nabla^2 V_{jl}(\mathbf{r}_1) = -e/(\epsilon\epsilon_0)\psi_j^*(\mathbf{r}_1)\psi_l(\mathbf{r}_1)$ with the boundary condition

$$V_{jl}(\mathbf{r}_b) = \frac{e}{4\pi\epsilon_0} \int d^3\mathbf{r}_1 \frac{\psi_j^*(\mathbf{r}_1)\psi_l(\mathbf{r}_1)}{\epsilon|\mathbf{r}_b - \mathbf{r}_1|}, \quad (13)$$

where \mathbf{r}_b lays within the boundary of the the computational box. The Poisson equation is solved on a grid that covers the dot area. The calculation accuracy is carefully monitored²⁶ and a configuration-interaction calculation convergence better than $10 \mu\text{eV}$ is reached for $n = 20$.

C. Parameters

The bulk of our results presented in the following sections are obtained for the parameters described below. In the experiment of Ref. 21, an anisotropic InAs self-organized quantum dot (SOQD) grown on a [001] GaAs substrate is studied with a confinement potential that is elongated due to the source and drain electrodes placed above the dot. The orientation of the dot with respect to the in-plane crystal

directions is not well resolved and in the present work, this is taken as an additional parameter that is studied. We take $R_x = 100 \text{ nm}$ as the long and $R_y = 60 \text{ nm}$ as the short size of the dot.²¹ We take $R_z = 10 \text{ nm}$ as a reasonable estimate of the dot height (note that the SOQD has a nominal pyramidal shape²¹ with height 20 nm , but our model is limited to a potential with a rectangular shape of vertical cross section). R_z influences the effective strength of the Dresselhaus-coupling constant and the orbital effects of the in-plane magnetic field. Results for $R_z > 10 \text{ nm}$ are also discussed below.

For the purpose of the present study, it is important to notice that the electric field in the growth direction defines the strength of the Rashba coupling. The electric field is influenced by the potential profile within the dot,²⁷ the Schottky barrier at the dot-electrode interface, surface charges, and the applied potentials.²⁴ The electrostatics of the actual device is complex and its complete description is out of the scope of the present work. Nevertheless, we are able to estimate the external electric field present in the system by considering the stability diagram and the width of the systems.²⁸ We estimated the maximal value of the external electric field to be of order -30 kV/cm , for which the electrons are still present in the dot.²⁹ From the gate voltage, $V_g = -0.4 \text{ V}$, of two-electron spectroscopy, we estimated $F_z = -13.6 \text{ kV/cm}$, and this value is used in our numerical calculation. Finally, in this paper we indicate that the ratio of the Rashba-coupling strength (that is proportional to F_z) to the strength of the Dresselhaus coupling can be extracted from the experimentally measured orientation of the magnetic field for which the SO-induced AC vanishes.

We take the SO coupling parameters as $\alpha = 1.1 \text{ nm}^2$, from Ref. 30, for the Rashba coupling and $\gamma = 26.9 \text{ meV nm}^3$, from Ref. 31, for the Dresselhaus coupling constant. The material parameters for InAs are adopted from Ref. 32, with values $m^* = 0.026$ and $g = -17.5$.

III. RESULTS

A. Without SO coupling

We consider first a dot aligned such that the x axis is oriented along [100] (y axis along [010]), namely, $\theta = 0$. The energy spectrum obtained in the absence of the SO coupling (we take $\alpha = \gamma = 0$) for a single-electron anisotropic quantum dot is presented in Fig. 2 by the black solid curves. In the absence of the magnetic field, the ground state is doubly degenerate with respect to spin and the spatial wave function is of even symmetry with respect to plane inversions: $\psi(x, y, z) = \psi(-x, y, z)$, $\psi(x, y, z) = \psi(x, -y, z)$, and $\psi(x, y, z) = \psi(x, y, -z)$. We denote the state of even symmetry with respect to all inversions by $|\psi_+\rangle$. The first excited state is a spin-doublet with wave functions meeting the symmetry conditions: $\psi(x, y, z) = -\psi(-x, y, z)$, $\psi(x, y, z) = \psi(x, -y, z)$, and $\psi(x, y, z) = \psi(x, y, -z)$. We will refer to this state as $|\Psi_-\rangle$. The nonzero magnetic field lifts the spin-degeneracy splitting of the states of the same parity by the Zeeman energy. The energy levels depicted by the black lines in Fig. 2 are obtained regardless of the ϕ value in spite of the lateral anisotropy of the dot. Due to the small R_z value and the

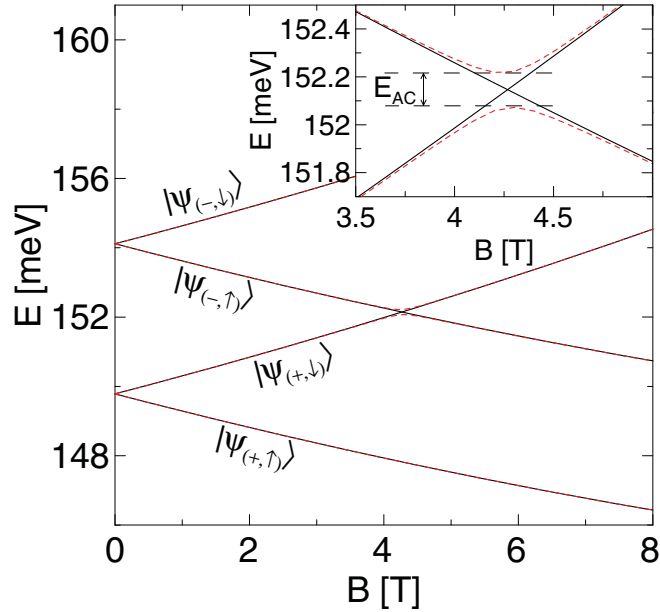


FIG. 2. (Color online) The black solid curves represent the one-electron-energy spectrum obtained without spin-orbit coupling for the in-plane magnetic field, regardless of the ϕ value. The red dashed curves are the energy levels when only Dresselhaus coupling with $\gamma = 26.9 \text{ meV nm}^3$ is included with the magnetic field aligned along the y direction ($\phi = 90^\circ$). The inset shows a zoom-in view of the energy levels in the vicinity of the anticrossing.

in-plane alignment of \mathbf{B} , no orbital effects of the magnetic field are observed (the influence of the height of the dot is studied in Sec. III F).

Generally, in the presence of an in-plane magnetic field, the Hamiltonian in Eq. (1), even without SO interaction, does not commute with the plane-inversion operators P_x and P_y [defined as $P_x f(x, y, z) = f(-x, y, z)$ and $P_y f(x, y, z) = f(x, -y, z)$]. However, due to the insignificance of the orbital effect of the magnetic field for this flat quantum dot, the parity with respect to reflection through the $x = 0$ and $y = 0$ planes is approximately preserved (with $\langle P_x \rangle$ and $\langle P_y \rangle$ above 0.97) even for nonzero B . For the following discussion, we denote the four lowest-energy states for a small magnetic field aligned parallel to the y direction as $|\Psi_{(+,\uparrow)}\rangle$, $|\Psi_{(+,\downarrow)}\rangle$, $|\Psi_{(-,\uparrow)}\rangle$, and $|\Psi_{(-,\downarrow)}\rangle$ with corresponding energies $E_{(+,\uparrow)}$, $E_{(+,\downarrow)}$, $E_{(-,\uparrow)}$, and $E_{(-,\downarrow)}$, where the arrow denotes the spin state aligned parallel (\uparrow) or antiparallel (\downarrow) to the magnetic-field vector.

B. Single type of SO coupling

Inclusion of the SO interaction lifts the spin polarization of the states and changes the crossing observed between the energy levels of $|\Psi_{(+,\downarrow)}\rangle$ and $|\Psi_{(-,\uparrow)}\rangle$ around $B = 4.25 \text{ T}$ into an anticrossing. The inset of Fig. 2 shows the anticrossing energy levels for $\phi = 90^\circ$ (\mathbf{B} parallel to the y axis) represented by the red curves when only Dresselhaus coupling with

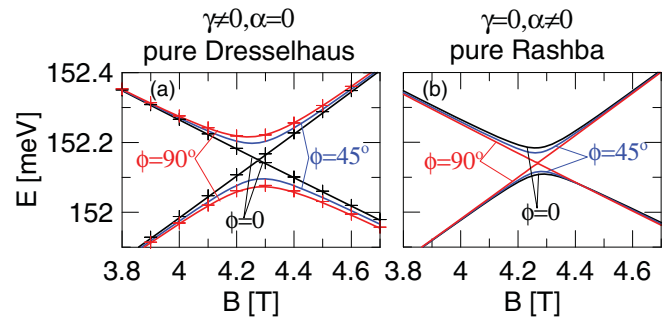


FIG. 3. (Color online) The energy levels near the anticrossing for pure Dresselhaus (a) and pure Rashba (b) couplings for different \mathbf{B} orientations. The black crosses are the results from a diagonalization of the matrix in Eq. (22) and the red crosses the results of diagonalization of Eq. (19). The magnetic field is oriented along the x direction ($\phi = 0$) for the black symbols and curves and along the y direction ($\phi = 90^\circ$) for the red symbols and curves.

$\gamma = 26.9 \text{ meV nm}^3$ is included. We denote the minimal energy difference between the anticrossing levels as E_{AC} . For the applied parameters, we obtain $E_{AC} = 146 \mu\text{eV}$. Outside the anticrossing the SO interaction does not modify the energy spectrum in a noticeable way, i.e., the black and red curves approximately coincide.

In the presence of the SO coupling, the anticrossing energy levels depend on the orientation of the magnetic field. In Figs. 3(a) and 3(b), we plot the energy levels obtained for pure Dresselhaus and pure Rashba interaction, respectively, for three different ϕ values. In both cases, clear dependence of the anticrossing width, E_{AC} , is observed with respect to the \mathbf{B} orientation. For pure Dresselhaus coupling the anticrossing is the widest when the magnetic-field vector is perpendicular to the y direction ($\phi = 90^\circ$) [the red curve in Fig. 3(a)]. When the field is aligned along the x direction ($\phi = 0$), the mixing between levels vanishes [the black curve in Fig. 3(a)] and there is crossing of the levels. With pure Rashba coupling the dependence is opposite; the anticrossing vanishes when \mathbf{B} is aligned along y , and E_{AC} is largest when \mathbf{B} is aligned along x .

The direction of the magnetic field for which the mixing between the states disappears can be inferred from the analytic form of the SO Hamiltonians utilizing the approximate symmetries of the wave functions of confined electron. Let us first inspect the case of pure Dresselhaus coupling and remind that for $\theta = 0$ the Hamiltonian in Eq. (4) has the same form in the x , y , and z coordinate system. Averaging the Hamiltonian in Eq. (4) over the z direction one obtains

$$H_{\text{BIA}}^{2\text{D}} = \gamma \langle k_z^2 \rangle [\sigma_x k_x - \sigma_y k_y] + \gamma [\sigma_y k_y k_x^2 - \sigma_x k_x k_y^2] + \gamma \sigma_z \langle k_z \rangle (k_y^2 - k_x^2). \quad (14)$$

The second term is the so-called cubic Dresselhaus term, which is negligible as long as the height is much smaller than the lateral size of the dot (i.e., until the value of $\langle k_x^2 \rangle$ or $\langle k_y^2 \rangle$ becomes comparable with $\langle k_z^2 \rangle$). For an infinite-quantum-well ground-state wave function in the z direction the last term in Eq. (14) vanishes³³ and

$$\gamma^{2\text{D}} = \gamma \langle k_z^2 \rangle = \gamma (\pi/R_z)^2. \quad (15)$$

The simplified Dresselhaus Hamiltonian takes now the following form:

$$H_{\text{BIA}}^{2\text{D}} = \gamma^{2\text{D}}(\sigma_x k_x - \sigma_y k_y). \quad (16)$$

$$\begin{pmatrix} E_{(+,\downarrow)} + \gamma^{2\text{D}} \langle \Psi_{(+,\downarrow)} | \sigma_x k_x - \sigma_y k_y | \Psi_{(+,\downarrow)} \rangle & \gamma^{2\text{D}} \langle \Psi_{(+,\downarrow)} | \sigma_x k_x - \sigma_y k_y | \Psi_{(-,\uparrow)} \rangle \\ \gamma^{2\text{D}} \langle \Psi_{(-,\uparrow)} | \sigma_x k_x - \sigma_y k_y | \Psi_{(+,\downarrow)} \rangle & E_{(-,\uparrow)} + \gamma^{2\text{D}} \langle \Psi_{(-,\uparrow)} | \sigma_x k_x - \sigma_y k_y | \Psi_{(-,\uparrow)} \rangle \end{pmatrix}. \quad (17)$$

The states $|\Psi_{(+,\downarrow)}\rangle$ and $|\Psi_{(-,\uparrow)}\rangle$ are separable into an orbital and spin part. Due to the action of the Pauli matrices on the states with a definite spin one gets

$$\begin{pmatrix} E_{(+,\downarrow)} - \gamma^{2\text{D}} \langle \Psi_{(+,\downarrow)} | \sigma_y k_y | \Psi_{(+,\downarrow)} \rangle & \gamma^{2\text{D}} \langle \Psi_{(+,\downarrow)} | \sigma_x k_x | \Psi_{(-,\uparrow)} \rangle \\ \gamma^{2\text{D}} \langle \Psi_{(-,\uparrow)} | \sigma_x k_x | \Psi_{(+,\downarrow)} \rangle & E_{(-,\uparrow)} - \gamma^{2\text{D}} \langle \Psi_{(-,\uparrow)} | \sigma_y k_y | \Psi_{(-,\uparrow)} \rangle \end{pmatrix}. \quad (18)$$

For the magnetic-field vector aligned parallel to the y direction, the components of the momentum-operator vector are $k_x = -i \frac{\partial}{\partial x} + eBz$, $k_y = -i \frac{\partial}{\partial y}$, and $k_z = -i \frac{\partial}{\partial z}$. Due to parity one obtains

$$\begin{pmatrix} E_{(+,\downarrow)} & -i \gamma^{2\text{D}} \langle \Psi_{(+,\downarrow)} | \sigma_x \frac{\partial}{\partial x} | \Psi_{(-,\uparrow)} \rangle \\ -i \gamma^{2\text{D}} \langle \Psi_{(-,\uparrow)} | \sigma_x \frac{\partial}{\partial x} | \Psi_{(+,\downarrow)} \rangle & E_{(-,\uparrow)} \end{pmatrix}. \quad (19)$$

The nonvanishing off-diagonal matrix elements mix the states $|\Psi_{(+,\downarrow)}\rangle$ and $|\Psi_{(-,\uparrow)}\rangle$, which results in an avoided crossing between the corresponding energy levels. By the red crosses

$$\begin{pmatrix} E_{(+,\leftarrow)} + \gamma^{2\text{D}} \langle \Psi_{(+,\leftarrow)} | \sigma_x k_x - \sigma_y k_y | \Psi_{(+,\leftarrow)} \rangle & \gamma^{2\text{D}} \langle \Psi_{(+,\leftarrow)} | \sigma_x k_x - \sigma_y k_y | \Psi_{(-,\rightarrow)} \rangle \\ \gamma^{2\text{D}} \langle \Psi_{(-,\rightarrow)} | \sigma_x k_x - \sigma_y k_y | \Psi_{(+,\leftarrow)} \rangle & E_{(-,\rightarrow)} + \gamma^{2\text{D}} \langle \Psi_{(-,\rightarrow)} | \sigma_x k_x - \sigma_y k_y | \Psi_{(-,\rightarrow)} \rangle \end{pmatrix}. \quad (20)$$

Due to spin one gets

$$\begin{pmatrix} E_{(+,\leftarrow)} + \gamma^{2\text{D}} \langle \Psi_{(+,\leftarrow)} | \sigma_x k_x | \Psi_{(+,\leftarrow)} \rangle & -\gamma^{2\text{D}} \langle \Psi_{(+,\leftarrow)} | \sigma_y k_y | \Psi_{(-,\rightarrow)} \rangle \\ -\gamma^{2\text{D}} \langle \Psi_{(-,\rightarrow)} | \sigma_y k_y | \Psi_{(+,\leftarrow)} \rangle & E_{(-,\rightarrow)} + \gamma^{2\text{D}} \langle \Psi_{(-,\rightarrow)} | \sigma_x k_x | \Psi_{(-,\rightarrow)} \rangle \end{pmatrix}. \quad (21)$$

For the magnetic field aligned along the x direction the components of the momentum operator vector are $k_x = -i \frac{\partial}{\partial x}$, $k_y = -i \frac{\partial}{\partial y}$, and $k_z = -i \frac{\partial}{\partial z} + eBy$. All integrals in Eq. (21) vanish due to the parity of the states and we finally obtain

$$\begin{pmatrix} E_{(+,\leftarrow)} & 0 \\ 0 & E_{(-,\rightarrow)} \end{pmatrix}. \quad (22)$$

Let us now consider the case of a magnetic field aligned parallel to the y direction and inspect matrix elements of the $H_{\text{BIA}}^{2\text{D}}$ Hamiltonian in a basis that include only the low-energy states $|\Psi_{+,\downarrow}\rangle$ and $|\Psi_{-,\uparrow}\rangle$ that exhibit an energy crossing without SO coupling. The matrix is given by

in Fig. 3 we plot numerically calculated eigenvalues of the matrix in Eq. (19). Note that the crosses and lines are in perfect agreement, proving that for our dot, with the assumed geometry, the $H_{\text{BIA}}^{2\text{D}}$ is, in fact, a good approximation to H_{BIA} .

Let us now consider the case of a magnetic field aligned parallel to the x ($\phi = 0$) direction. In this case, the low-energy states, for which energy levels cross without SO coupling, are $|\Psi_{(+,\leftarrow)}\rangle$ and $|\Psi_{(-,\rightarrow)}\rangle$, where the arrow denotes the electron spin aligned parallel (\rightarrow) and antiparallel (\leftarrow) to the magnetic-field vector, \mathbf{B} . The matrix of the $H_{\text{BIA}}^{2\text{D}}$ Hamiltonian in this two-state basis is

The matrix in Eq. (22) consists only of diagonal elements that are equal to the energy of the basis states. Thus the $|\Psi_{(+,\leftarrow)}\rangle$ and $|\Psi_{(-,\rightarrow)}\rangle$ states are not mixed by the Dresselhaus coupling in this configuration and there is no anticrossing of energy levels. We plot the eigenvalues of the matrix in Eq. (22) in Fig. 3(a) (represented by the black crosses).

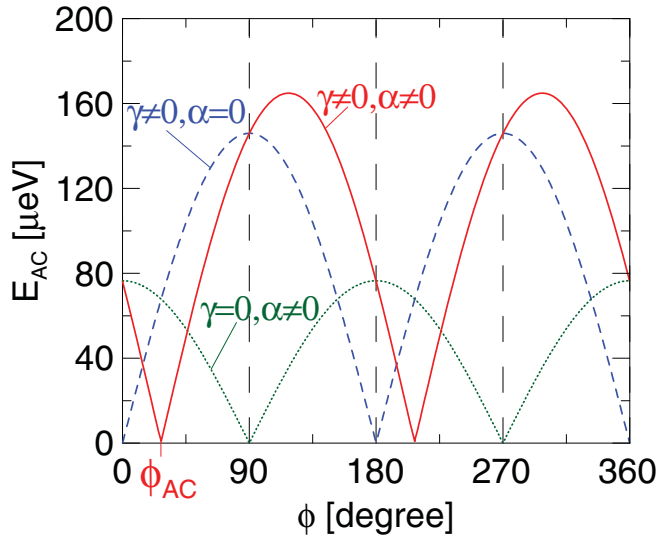


FIG. 4. (Color online) The spin-orbit-induced anticrossing width, E_{AC} , for pure Dresselhaus (blue dashed curve), pure Rashba (green dotted curve), and both (red solid line) interactions present. For $\gamma = 0$ the magnetic field is $B = 4.268$ T, for the two other cases, $B = 4.277$ T.

A similar analysis can be made for the Rashba Hamiltonian given by Eq. (2). Due to the fact that the analytic form of both Hamiltonians H_{SIA} and H_{BIA}^{2D} is similar, i.e., only the k_x and k_y are swapped (and the coupling constants are different), it is clear that the dependence of AC width on the magnetic-field direction is reversed, i.e., the mixing between the states vanishes when the magnetic field is aligned along the y direction.

C. Anisotropy in the presence of both SO couplings

Let us now consider the effect of both Dresselhaus and Rashba couplings. Figure 4 presents the avoided-crossing energy, E_{AC} , as a function of the angle ϕ between the x axis and the magnetic field. For pure Dresselhaus (the blue dashed curve in Fig. 4) and pure Rashba (the green dotted curve in Fig. 4) coupling the extrema are shifted by 90° , in agreement with our previous analysis. The curves in Fig. 4 are accurately described by $|\sin(\phi - \phi_{AC})|$, which is the same functional form as the one observed in the experimental work of Ref. 21 in Fig. 3(f) (where the behavior was described by $|\cos(\phi - \phi_0)|$). Moreover, the maximal value of E_{AC} is of the same order as the magnitude observed experimentally. When both SO interactions are present, the dependence of the anticrossing width is plotted in Fig. 4 by the red curve. The shape of the latter is the same as for pure Dresselhaus or Rashba coupling, with pronounced minima where E_{AC} is equal to zero. When the magnetic field is aligned along the x or y direction, the E_{AC} equals to the value for pure SO coupling. Note that the maxima are larger than the ones observed for pure couplings and its positions are now shifted and are no longer aligned along the axes of the dot. For $\alpha = 1.1 \text{ nm}^2$ and $\gamma = 26.9 \text{ meV nm}^3$, the shift of the dependence is $\phi_{AC} = 27.8^\circ$. The latter value can be understood as follows. Let us denote the direction of the magnetic field for which the AC vanishes for pure Dresselhaus and pure Rashba couplings by the vectors \mathbf{d}_{BIA} and \mathbf{d}_{SIA} ,

respectively. Next, we estimate the strength of each interaction. The maximal induced anticrossing width is $E_{AC}^{BIA} = 146 \mu\text{eV}$ and $E_{AC}^{SIA} = 77 \mu\text{eV}$ for Dresselhaus and Rashba coupling, respectively. Thus the Dresselhaus interaction is 1.9 times larger than the Rashba coupling, which makes the vector \mathbf{d}_{BIA} 1.9 times longer than \mathbf{d}_{SIA} . Let us denote the magnetic field for which the effect of both spin-orbit couplings is zero by the vector $\mathbf{d}_{BIA+SIA} = \mathbf{d}_{BIA} + \mathbf{d}_{SIA}$. It is easy to show that this vector forms an angle $\phi = 27.8^\circ$ with the x axis. Thus when both couplings are present, the effect of the total spin-orbit coupling disappears when the external magnetic field is directed along this vector. In fact, that is exactly what we observe in our calculation (see position of the minimum of the dependence depicted with the red curve in Fig. 4). The formula $|\sin(\phi - \phi_{AC})|$ reflects the fact that the dependency obtained for both SO couplings present can be considered as an absolute value of a sum of the dependencies obtained for pure SO couplings, described by $-\cos\phi$ and $\sin\phi$ for pure Rashba and Dresselhaus couplings, respectively.

D. Dependence on the quantum dot orientation

Different in-plane orientations of the anisotropic potential of the dot with respect to the crystal host where the long axis of the dot forms an angle θ with $[100]$ are now considered. In Figs. 5(a)–5(c), we present the size of the AC as a function of the direction of the rotated magnetic field (note that the ϕ angle is defined as an angle between the magnetic-field vector and the long axis of the dot) for six different orientations of the dot. The dotted curves in Fig. 5(a) represent the result obtained for pure Rashba coupling. We observe that the E_{AC} dependencies are exactly the same as in Fig. 4 regardless of the dot alignment. The minimum of the E_{AC} does not change its position and the energy levels are not affected by the orientation of the dot. With the green diamonds we show, in Fig. 5(d), the ϕ_{AC} angle for which the $E_{AC} = 0$ as a function of the angle θ .

For pure Dresselhaus coupling, the E_{AC} dependencies [depicted by dashed curves in Fig. 5(b)] are shifted as the dot is rotated. For the case studied in the previous subsections

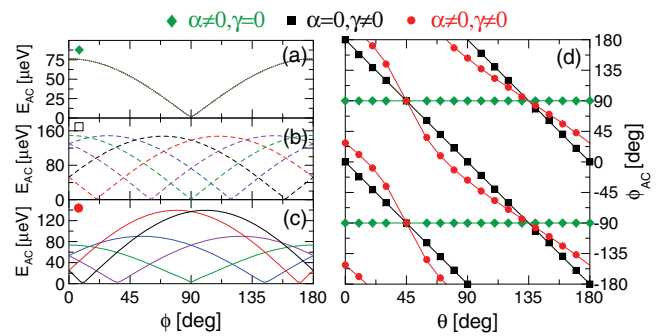


FIG. 5. (Color online) Avoided-crossing-energy width as a function of the direction (ϕ) for different orientations of the dot with $\theta = 10^\circ$ (black curves), 30° (blue curves), 45° (green curves), 60° (violet curves), and 80° (red curves). Results are shown for (a) pure Rashba, (b) pure Dresselhaus and (c) for both couplings present. (d) The value of the magnetic-field angle, ϕ_{AC} , at which $E_{AC} = 0$ as a function of the angle θ for pure Rashba (green diamonds), pure Dresselhaus (black squares), and both couplings present (red dots). The red curves are obtained from Eq. (23).

(where $\theta = 0$), the AC vanished when the magnetic field was aligned along the long axis of the dot ($\phi_{AC} = 0$). When the dot is oriented so that $\theta = 45^\circ$ (long axis oriented along the [110] direction), the anticrossing vanishes when the magnetic field is aligned along the short axis of the dot [see green dashed curve in Fig. 5(b)]. For $\phi_{AC} = 90^\circ$, the same behavior was observed as in pure Rashba case. We plot in Fig. 5(d) the angle ϕ_{AC} for pure Dresselhaus coupling (the black squares) for different orientations of the dot. We find that the angle exhibits a $\phi_{AC} = -2\theta$ dependence [black solid lines in Fig. 5(d)]. Moreover, we observe that for both cases, when only a single type of SO coupling is present the maximal value of the AC width remains unchanged.

In Fig. 5(c), we show the results when both SO couplings are present (the solid curves). The maximal values of E_{AC} and the angle ϕ_{AC} for which the minima are observed change when the dot orientation is varied. Both facts can be understood similarly as discussed in Sec. III C. We can justify the ϕ_{AC} values considering the orientation of the $\mathbf{d}_{BIA+SIA} = \mathbf{d}_{BIA} + \mathbf{d}_{SIA}$ vector. But now the orientation of the \mathbf{d}_{BIA} vector, assigned to the Dresselhaus coupling, is changed as the dot is rotated, i.e., \mathbf{d}_{BIA} forms an angle -2θ with the long axis of the dot. The rotation of the dot does not change the maximal value of E_{AC} when only a single type of SO coupling is present, and the previously derived value for the relative strength of both couplings remains unchanged (and thus also the ratio of the length of the \mathbf{d}_{BIA} and \mathbf{d}_{SIA} vectors). We take 1 as the length of \mathbf{d}_{SIA} and 1.9 as the length of \mathbf{d}_{BIA} . In Fig. 6, we schematically present the considered vectors and the angles they form with the axes of the dot. The angle between the $\mathbf{d}_{BIA+SIA}$ vector (see red arrow in Fig. 6) and the x direction can be easily calculated

$$\phi_{AC} = \arctan \left[\frac{1 + 1.9 \sin(-2\theta)}{1.9 \cos(2\theta)} \right]. \quad (23)$$

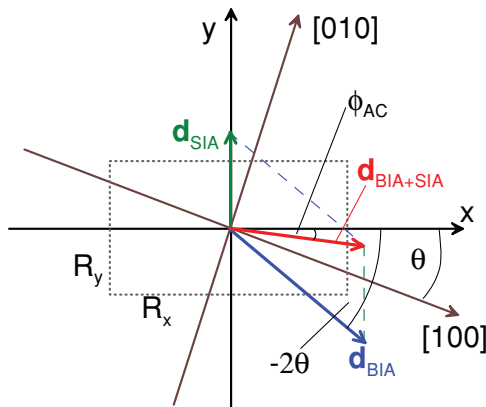


FIG. 6. (Color online) Schematics of the method of calculation of the angle ϕ_{AC} for which the AC vanishes when both SO couplings are present and the quantum dot (dashed rectangle) is oriented with its long axis forming an angle θ with the [100] direction. The vectors depict the directions of \mathbf{B} for which $E_{AC} = 0$ for pure Rashba coupling (green arrow), pure Dresselhaus coupling (blue arrow), and both couplings present (red arrow). The coordinate system connected with the dot axes and the crystallographic directions is also shown.

With the red dots in Fig. 5(d) we plot the angle ϕ_{AC} obtained from our numerical calculation in the presence of both couplings for different orientations of the dot, which agree very well with the values (red curves) obtained from Eq. (23). Along with the changes of the orientation, the length of the $\mathbf{d}_{BIA+SIA}$ vector is changed, which results in the different values of the maximal AC width observed in Fig. 5(c).

A systematic study of the value of the ϕ_{AC} angle dependence on the SO coupling strengths and the dot alignment is given in Sec. III G where the two-electron case is studied.

E. Quantum dot with a square base

The above discussion was for a lateral anisotropic quantum dot. Now we study the case of a dot with a symmetrical base (we assume $R_x = R_y = 100$ nm) and $\theta = 0$, and we investigate if this has an influence on the anisotropy induced by the SO coupling. In the absence of the SO interaction and a magnetic field, the first-excited state is spin-doubly degenerate due to parity. The magnetic field lifts the spin degeneracy but the degeneracy due to parity is not removed. The inclusion of a single type of SO interaction induces a repulsion between the energy levels of the ground-state and one of the states from the parity doublet [see the red dashed curves in Fig. 7(a) for the case of pure Dresselhaus coupling and Fig. 7(b) for pure Rashba coupling]. The same configuration of energy levels is obtained regardless of the angle ϕ . In both Figs. 7(a) and 7(b), the black ($\phi = 0$), blue ($\phi = 45^\circ$), yellow dotted ($\phi = 22.5^\circ$), and red dashed curves ($\phi = 90^\circ$) coincide. The dependence of the energy levels on the magnetic-field orientation starts to appear already when the dot is elongated by a factor of 1%.

However, when both Rashba and Dresselhaus interactions are present the AC width varies with the rotation of the magnetic field, see Figs. 7(c) and 7(d). We observe that the anisotropy is most pronounced when α is increased by a factor of two—the case when both couplings have comparable strengths.^{23,34} In such a case, when the magnetic field is directed along the diagonal, i.e., $\phi = 45^\circ$ [see blue curves

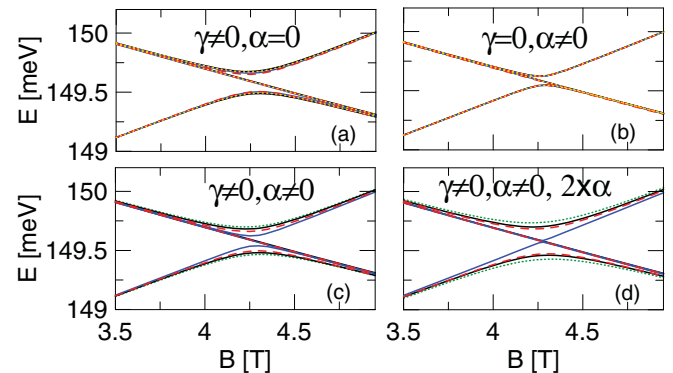


FIG. 7. (Color online) Energy levels of one-electron quantum dot with a square base with $R_x = R_y = 100$ nm. The black curves correspond to $\phi = 0$, the blue curves to $\phi = 45^\circ$, yellow dotted to $\phi = 22.5^\circ$, and the red dashed curves to $\phi = 90^\circ$. In (c) and (d), we additionally plot the energy levels obtained for $\phi = 135^\circ$ with green dotted curves. (a) Pure Dresselhaus coupling, (b) pure Rashba interaction, (c) both SO interactions are present, and (d) both SO interactions are present with α increased by a factor of two.

in Fig. 7(d)] the anticrossing between the energy levels of the ground state and both states from the parity doubled becomes very small.

F. Larger dot height

Let us now return to the case of the quantum dot with a rectangular base with $R_x = 100$ nm and $R_y = 60$ nm. For the previous dot with $R_z = 10$ nm no orbital effects from the magnetic field on the energy spectrum were observed [see the black curves in Fig. 2]. However, this is no longer true for larger R_z values. This can be seen from Figs. 8(a) and 8(b) where we plot the energy levels of a quantum dot with height $R_z = 20$ nm and $R_z = 40$ nm, respectively, in the presence of SO coupling (with both SO interactions present). The energy levels depend on the magnetic-field orientation even outside the anticrossing region. This is due to the elongation of the confinement potential in the x direction. The SO-induced anticrossing is shifted to lower magnetic fields as the value of the angle ϕ becomes closer to $\phi = 90^\circ$ [this is analogous to the experimental observation—compare with Fig. S7(a) from Ref. 28]. We calculated the anticrossing widths for different values of ϕ and we plot them as red dots in the insets of Fig. 8. Then we fitted the points with the function $A|\sin(\phi - \phi_{AC})|$, where $A = 86 \mu\text{eV}$ and $\phi_{AC} = 65^\circ$ for $R_z = 20$ nm and $A = 77 \mu\text{eV}$ and $\phi_{AC} = 82^\circ$ for $R_z = 40$ nm. Notice the agreement between the fitted curve and the data points. From this fact we conclude that in spite of the presence of orbital effects, the previously found dependence of the anticrossing width on the angle ϕ still holds, but with modified A and ϕ_{AC} values. The latter fact can be attributed to the reduction of the Dresselhaus coupling strength. This can be accounted for by considering the Dresselhaus coupling Hamiltonian in Eq. (16), in which the coupling strength decreases as $(1/R_z)^2$. In the calculation performed for pure Dresselhaus interaction, we obtain the maximal E_{AC} values: 146, 37, and 11 μeV for $R_z = 10, 20,$ and 40 nm, respectively—the obtained E_{AC} values decrease approximately as $(1/R_z)^2$ with the largest discrepancy for large R_z values (i.e., when the approximation of the coupling strength by Eq. (15) becomes inaccurate). The decrease of the Dresselhaus-coupling strength with increasing height of the dot results in a shift of the E_{AC} dependency on ϕ toward the one obtained for a flat quantum-dot with only Rashba interaction present compare the black curve in the inset of Fig. 8(b) with the green dotted curve in Fig. 4— ϕ_{AC} becomes close to 90° . Also the maximal E_{AC} value becomes closer to the one obtained for pure Rashba coupling— A tends to 77 μeV with increasing R_z . The shift in the ϕ_{AC} value [see insets of Figs. 8(a) and 8(b)] can be understood from the relative strengths of the Rashba and Dresselhaus couplings as discussed in Sec. III C.

G. Two-electron results

In a recent experiment [21], the ground state and excited states were measured provided that the latter entered into a finite but narrow transport window determined by the voltages applied to the source and drain electrodes. The avoided crossings that appear for a single-electron in the excited part

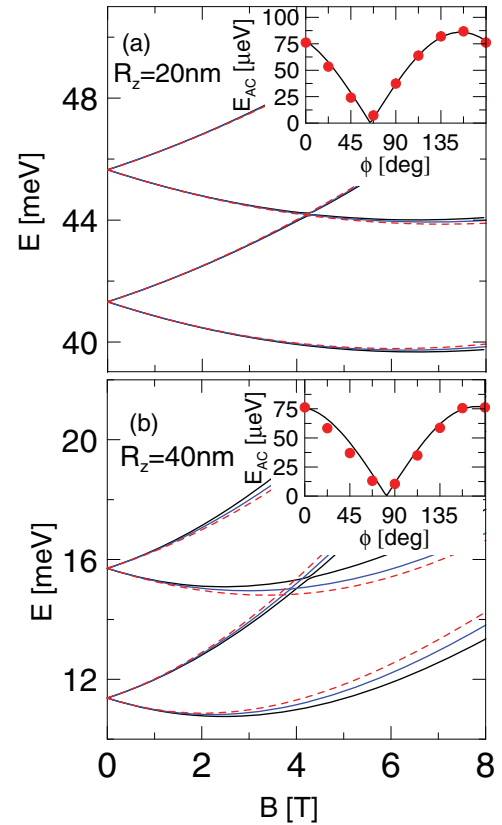


FIG. 8. (Color online) One-electron energy levels for a rectangular-based quantum dot with (a) $R_z = 20$ nm and (b) $R_z = 40$ nm for $\phi = 0, 45^\circ,$ and 90° plotted with the black solid, blue solid, and red dashed curves, respectively. The red dots in the insets of both plots present the anticrossing width, E_{AC} obtained from the energy spectrum for a given ϕ value; the black curves are the fitted $|\sin(\phi - \phi_{AC})|$ dependencies.

of the spectrum, which we described above, were outside the transport window.

In the two-electron regime and in the absence of both the magnetic field and the SO interaction, the ground state is a spin singlet and the first excited state is a spin triplet. Under the presence of an external magnetic field the ground-state singlet energy crosses the triplet energy. When we turn on the SO coupling it induces an avoided crossing between the states of opposite spin which was well resolved in the experiment [21].

Similarly to the one-electron case, the SO coupling is responsible for changes in the size of the anticrossing energy when the orientation of the magnetic field is varied. Figure 9 presents the low-energy spectrum of the two-electron quantum dot in the presence of both Rashba and Dresselhaus couplings for a dot aligned with its long axis along the [100] direction ($\theta = 0$). In the inset, we plot the energy levels in the vicinity of the AC. The anticrossing vanishes for exactly the same angle, $\phi_{AC} = 27.8^\circ$, as for the one-electron case discussed above (see the green curves in the inset of Fig. 9).

In Fig. 10(a), we plot the angular dependence of the anticrossing width, E_{AC} , for pure Dresselhaus, pure Rashba, and when both couplings are present by the blue dashed, green dotted, and solid red curves, respectively. Notice that all three

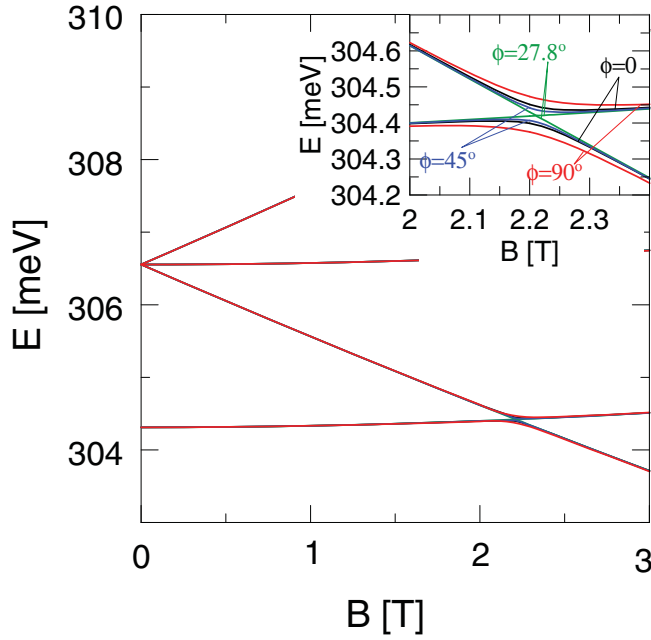


FIG. 9. (Color online) Two-electron energy spectrum in the presence of both Rashba and Dresselhaus SO coupling for angles $\phi = 0$ (black curves), 27.8° (green curves), 45° (blue curves), and 90° (red curves). The inset shows the energy levels in the vicinity of the anticrossing. The results are obtained for $\theta = 0$.

dependencies have the same shape as for the case of the one electron considered in Sec. III B (compare with Fig. 4), only the maximal E_{AC} values are about 1.5 times smaller.

As was presented in Sec. III C, for the anisotropic quantum dot the angle ϕ_{AC} depends on the relative strength of both SO interactions and the in-plane orientation of the dot (explained in Sec. III D). On the other hand, the ϕ_{AC} value can be measured experimentally²¹ and the orientation of the quantum dot with respect to the crystal directions can be obtained by inspecting the facets of the dot. This opens the possibility to employ such a measurement to evaluate the relative strength of the Rashba and Dresselhaus couplings for a dot with a given orientation with respect to the crystal host. Let us define the strength ratio of the SO interactions as the ratio of the effective coupling constants α^* and γ^{2D} . The Rashba coupling strength denoted with α^* is calculated as $\alpha^* = \alpha \left[\frac{\partial V}{\partial z} \right] = -\alpha |e| F_z$ and the Dresselhaus coupling γ^{2D} is obtained from Eq. (15).

We previously derived the angle ϕ_{AC} for given relative strength of the SO couplings for a given orientation of the dot [see Eq. (23)]. Let us substitute the $1/1.9$ value by α^*/γ^{2D} in Eq. (23) from which we obtain

$$\frac{\alpha^*}{\gamma^{2D}} = -\frac{\alpha}{\gamma} \frac{|e| F_z R_z^2}{\pi^2} = \cos(2\theta) [\tan(\phi_{AC}) - \tan(-2\theta)]. \quad (24)$$

This function is shown in Fig. 10(b) by the solid lines for different orientations of the quantum dot. With the black symbols we mark the angle ϕ_{AC} obtained from our numerical calculations for dots with different geometries (see Fig. 10 caption) with $\theta = 0$ for different SO coupling strengths. For such a case, with $\theta = 0$ (the dot oriented with its long axis along [100]) and pure Dresselhaus coupling ($\alpha^*/\gamma^{2D} = 0$) we obtain $\phi_{AC} = 0$. When the Rashba-coupling strength is

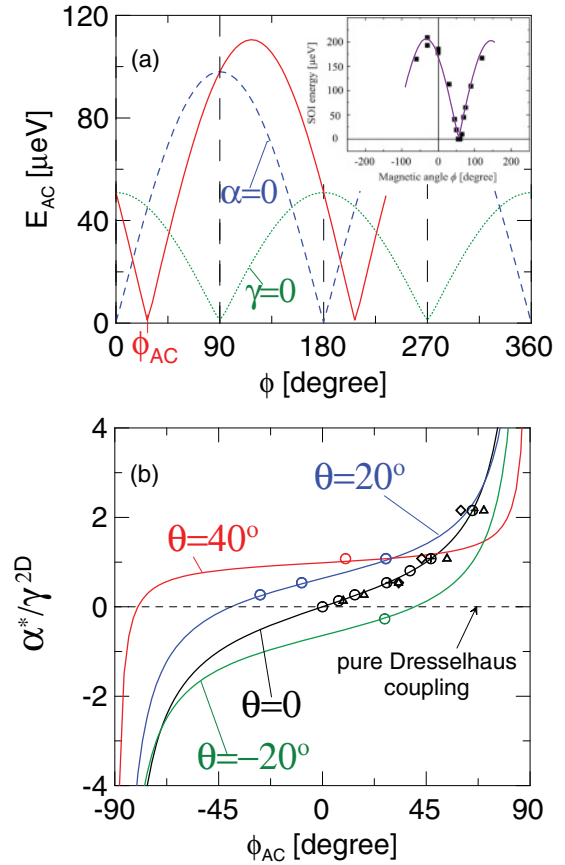


FIG. 10. (Color online) (a) Width of the singlet-triplet avoided crossing as a function of the angle ϕ for pure Dresselhaus coupling (blue dashed curve), pure Rashba coupling (green dotted curve), and for both couplings present (red solid curve). The inset shows the experimental results (symbols) of Ref. 21 together with the results of the present calculation (purple curve) with $\gamma = 29.58 \text{ meV nm}^3$ and $\alpha = 4.731 \text{ nm}^2$. The magnetic field is $B = 2.211 \text{ T}$ for pure Rashba coupling and $B = 2.209 \text{ T}$ for all the other cases. The dot is aligned with its long axis along [100], i.e., $\theta = 0$. (b) The ϕ_{AC} value for different strength ratios of the Rashba and Dresselhaus couplings for four different orientations of the dot. The symbols present the results of our numerical calculation and the curves represent the analytical result given by Eq. (24). The circles show the results obtained for $R_y = 60 \text{ nm}$ and $R_z = 10 \text{ nm}$, the crosses for $R_y = 30 \text{ nm}$ and $R_z = 10 \text{ nm}$, the triangles for $R_y = 20 \text{ nm}$ and $R_z = 10 \text{ nm}$, and the diamonds for $R_y = 60 \text{ nm}$ and $R_z = 20 \text{ nm}$. In all cases, R_x is 100 nm .

increased, the points move toward the angle $\phi_{AC} = 90^\circ$ obtained for pure Rashba SO coupling. The green, red, and blue symbols in Fig. 10(b) are the ϕ_{AC} values obtained from our two-electron numerical calculation for different orientations of the quantum dot.

In the above discussion, we assume that $\alpha^* = -\alpha |e| F_z$ and $\gamma^{2D} = \gamma \pi^2 / R_z^2$ describe the strength of the spin-orbit interactions. For the Rashba coupling, given by the Hamiltonian in Eq. (3) (i.e., when an electric field is only present in the growth direction), the above α^* expression is valid regardless of the dot geometry. However, due to the fact that γ^{2D} originates from the Hamiltonian in Eq. (14), it describes the strength of the Dresselhaus coupling correctly only when

TABLE I. Calculated strength ratios of the SO couplings for $\phi_{AC} = 59^\circ$ and different orientations of the dot.

θ	α^*/γ^{2D}
0	1.66
40°	1.27
45°	...
75°	-0.94
90°	-1.66

the cubic term, $\gamma[\sigma_y k_y k_x^2 - \sigma_x k_x k_y^2]$, is negligible, which is the case when $R_x, R_y \gg R_z$ and the term with $\langle k_z \rangle$ is close to zero, i.e., for a dot with limited height.³³ All the symbols in Fig. 10(b) approximately coincide with the dependency given by Eq. (24). A discrepancy is seen in the limit of a narrow dot with $R_y = 20$ nm (the triangles) and for increased height of the dot for $R_z = 20$ nm (diamond symbols). We conclude that for anisotropic quantum dots with limited height the α^*/γ^{2D} ratio is a good measure of the relative strength of the Rashba and Dresselhaus spin-orbit couplings, which can be estimated from the analytic expression in Eq. (24).

The experiment of Ref. 21 found $\phi_{AC} = 59^\circ$, and we can use Eq. (24) to calculate the relative strength of the SO interactions. However, as the orientation of the anisotropic potential of the dot with respect to the crystal directions was not resolved in the experiment we need to assume a value for θ . We take $\theta = 0$ and by matching the absolute value of the SO-coupling constants (through the maximal value of E_{AC}) we obtained $\alpha^*/\gamma^{2D} \simeq 1.66$ by fitting the experimentally measured values for the AC width with our simulation results. In the inset to Fig. 10(a), we plot our results (purple curve) for the SO-coupling constants $\gamma = 29.58$ meV nm³ and $\alpha = 4.731$ nm² together with the data points from Ref. 21. However, as the relation between the crystal directions and the long axis of the dot is not known, the fit only proves the validity of the discussed process behind the anisotropy and not the exact value of the ratio α^*/γ^{2D} . Moreover, as the electrostatics of the actual device is complex the presented result is not the *exact* simulation of the experiment. Therefore, we present in Table I the strength ratios for different orientations of the dot. Note that Eq. (24) does not allow us to calculate the relative strength of the couplings for a dot aligned with long axis exactly along [110] or [1 $\bar{1}$ 0]. In such a configuration, for pure Dresselhaus as well as for pure Rashba coupling the AC vanishes for $\phi_{AC} = 90^\circ$ [compare dotted curves in Fig. 5(a) with green dotted curve in Fig. 5(b)] and because of that, for both couplings present simultaneously the minimum of the E_{AC} dependence on ϕ is not shifted irrespective of the coupling strength ratio.

IV. DISCUSSION

In the present paper we discussed the avoided crossings of energy levels induced by the presence of different SO couplings. Only for the case of a square-based quantum-dot [see Figs. 7(a) and 7(b)] the dependence of AC width on the magnetic-field direction was observed solely for both couplings present with comparable strength. This result is related to those of Ref. 23 where the spin-splitting of

single-electron energy levels in strictly *two*-dimensional *circular* quantum dots in the presence of a *small* in-plane magnetic field (before the crossings and avoided crossings appear) was calculated. When the Dresselhaus- and Rashba-coupling strengths are equal, a well-known high-symmetric case is found, which is beneficial for many spintronic applications.^{5,10} For that special case, the energy spectrum is not affected by SO-interaction effects and the spin in the [110] direction is strictly defined. The Zeeman interaction lifts this symmetry and results in a spectrum that depends on the orientation of the magnetic field as discussed in Ref. 23. Since for equal coupling strengths the spins in the [110] direction are well defined, the Zeeman interaction for \mathbf{B} oriented along [110] does not produce any AC between energy levels of spin-orthogonal states [see the blue curve in Fig. 7(d)].

On the other hand, in the presence of a vertically oriented magnetic field, the size of the Zeeman interaction induced lifting of the symmetry depends on the in-plane orientation³⁴ and also on the width³⁵ of the dot, which results in changes of both the AC width and the effective g factor, which are solely observed when both SO interactions are present with a comparable strength. However, changing the dot orientation is hardly achievable experimentally and therefore, in the present work, we considered an anisotropy that can be probed by changing the orientation of the magnetic field.

In the present work, we investigated the anisotropic dependence of the avoided-crossing width that occurs even for a single type of SO coupling [see Figs. 3(a) and 3(b)]. This effect is strictly connected to both the elongation of the confinement potential and the in-plane alignment of the magnetic field (see the discussion in Sec. III B). The exact shape of the confinement potential is not important for the studied phenomena, which is a generic propriety of a spin-orbit-coupled quantum dot. In our analysis, we indicated the trends that determined the dependence of E_{AC} on ϕ , in particular, the dependence on the dot geometry [for the dot with increased height and for different lateral sizes of the dot the black symbols in Fig. 10 still undergo the same analytical dependence Eq. (24) in spite of the different geometries of the dot] or the orientation of the quantum dot with respect to the crystallographic directions (which influences the position of the minima of E_{AC} purely due to Dresselhaus coupling—see discussion in Sec. III D).

The present study shows that for an elongated quantum dot with pure Rashba coupling the anticrossing vanishes always when the magnetic field is aligned along the short axis of the dot [see the minima of the dotted curves in Figs. 4 and 5(a), and 10(a)]. Only the presence of Dresselhaus coupling can result in a ϕ_{AC} value that is different from 90° . The magnetic-field direction ($\phi_{AC} = 59^\circ$) for which the anticrossing vanished in the experiment of Ref. 21 suggests that both SO couplings are present, contrary to the argumentation provided in Ref. 21. The authors suggested that the Dresselhaus coupling would not induce mixing between the two lowest-energy states due to their well-defined and different values of the total angular momentum $J_- = L - S$ in a high magnetic field. However, we found that due to the in-plane alignment of the magnetic field³⁶ the Dresselhaus coupling, in fact, induces avoided crossings in the energy spectrum of a flat quantum dot [see

Fig. 2] and leads also to a shift in the dependence of the AC width on the magnetic-field direction [see Figs. 3, 5(a), 5(b), and 8].

V. SUMMARY AND CONCLUSIONS

We presented a study of the energy spectrum of one and two-electron spin-orbit-coupled three-dimensional quantum dots in the presence of an external in-plane magnetic field. We found that the size of the avoided crossings in the one- and two-electron energy spectrum oscillates as a function of the orientation of the magnetic field. The oscillatory behavior could accurately be described by $|\sin(\phi - \phi_{AC})|$, which agrees with recent excited-state-spectroscopy measurements performed on an InAs gated self-organized quantum dot.²¹

For a quantum dot that is elongated in the [100] direction, and when only a single type of SO coupling is present, the avoided crossing vanishes for $\phi_{AC} = 0$ ($\phi_{AC} = 90^\circ$), i.e., when the magnetic field is aligned parallel to the long (short) axis of the dot for Dresselhaus (Rashba) coupling. We explain this behavior as a consequence of parity and spin-dependent mixing of the states caused by the SO interaction. When both couplings are present the ϕ_{AC} value varies between 0 and

90° and the ratio of the relative strength of the interactions follows a $\tan(\phi_{AC})$ dependence. The change of the in-plane dot orientation results in a change of ϕ_{AC} , which is observed only when the Dresselhaus coupling is present. We show that the experimentally measured ϕ_{AC} value²¹ along with the knowledge of the orientation of the dot can be used to determine the ratio of the strengths of the individual SO interactions in the case of anisotropic quantum dots.

ACKNOWLEDGMENTS

The authors thank S. Takahashi for helpful discussions. This work was supported by the ‘‘Krakow Interdisciplinary PhD Project in Nanoscience and Advanced Nanostructures’’ operated within the Foundation for Polish Science MPD Programme co-financed by the EU European Regional Development Fund, the Project No. N N202103938 supported by the Ministry of Science and Higher Education (MNiSW) for 2010–2013, and the Belgian Science Policy (IAP). W. J. P. has been partially supported by the EU Human Capital Operation Program, Polish Project No. POKL.04.0101-00-434/08-00. Calculations were performed in ACK–CYFRONET–AGH on the RackServer Zeus.

¹K. C. Nowack, F. H. L. Koppens, Yu. V. Nazarov, and L. M. K. Vandersypen, *Science* **318**, 1430 (2007).

²S. Nadj-Perge, S. M. Frolov, E. P. A. M. Bakkers, and L. P. Kouwenhoven, *Nature (London)* **468**, 1084 (2010).

³E. Ya. Sherman and D. J. Lockwood, *Phys. Rev. B* **72**, 125340 (2005).

⁴S. Z. Denega, T. Last, J. Liu, A. Slachter, P. J. Rizo, P. H. M. van Loosdrecht, B. J. van Wees, D. Reuter, A. D. Wieck, and C. H. van der Wal, *Phys. Rev. B* **81**, 153302 (2010).

⁵B. A. Bernevig, J. Orenstein, and S. C. Zhang, *Phys. Rev. Lett.* **97**, 236601 (2006); J. D. Koralek, C. Weber, J. Orenstein, A. Bernevig, S. Zhang, S. Mack, and D. Awschalom, *Nature (London)* **458**, 610 (2009).

⁶M. Scheid, M. Kohda, Y. Kunihashi, K. Richter, and J. Nitta, *Phys. Rev. Lett.* **101**, 266401 (2008).

⁷L. Meier, G. Salis, E. Gini, I. Shorubalko, and K. Ensslin, *Phys. Rev. B* **77**, 035305 (2008); L. Meier, G. Salis, I. Shorubalko, E. Gini, S. Schön, and K. Ensslin, *Nat. Phys.* **3**, 650 (2007).

⁸S. Bednarek and B. Szafran, *Phys. Rev. Lett.* **101**, 216805 (2008); P. Földi, O. Kálmán, M. G. Benedict, and F. M. Peeters, *Nano Lett.* **8**, 2556 (2008); P. Földi, B. Molnár, M. G. Benedict, and F. M. Peeters, *Phys. Rev. B* **71**, 033309 (2005).

⁹S. Datta and B. Das, *Appl. Phys. Lett.* **56**, 665 (1990).

¹⁰J. Schliemann, J. C. Egues, and D. Loss, *Phys. Rev. Lett.* **90**, 146801 (2003).

¹¹K. V. Kavokin, *Phys. Rev. B* **64**, 075305 (2001); **69**, 075302 (2004); S. C. Bădescu, Y. B. Lyanda Geller, and T. L. Reinecke, *ibid.* **72**, 161304 (2005); S. Gangadharaiah, J. Sun, and O. A. Starykh, *Phys. Rev. Lett.* **100**, 156402 (2008).

¹²D. Loss and D. P. DiVincenzo, *Phys. Rev. A* **57**, 120 (1998).

¹³M. P. Nowak and B. Szafran, *Phys. Rev. B* **82**, 165316 (2010).

¹⁴G. Dresselhaus, *Phys. Rev.* **100**, 580 (1955).

¹⁵Y. A. Bychkov and E. I. Rashba, *J. Phys. C* **17**, 6039 (1984).

¹⁶D. V. Bulaev and D. Loss, *Phys. Rev. B* **71**, 205324 (2005); L. Meza-Montes, C. F. Destefani, and S. E. Ulloa, *ibid.* **78**, 205307 (2008); F. Qu, G. L. Iorio, V. Lopez-Richard, and G. E. Marques, *Appl. Phys. Lett.* **95**, 083101 (2009); M. P. Nowak and B. Szafran, *Phys. Rev. B* **81**, 235311 (2010); F. Baruffa, P. Stano, and J. Fabian, *ibid.* **82**, 045311 (2010); S. Nadj-Perge, S. M. Frolov, J. W. W. van Tilburg, J. Danon, Yu. V. Nazarov, R. Algra, E. P. A. M. Bakkers, and L. P. Kouwenhoven, *ibid.* **81**, 201305(R) (2010).

¹⁷K. Shen and M. W. Wu, *Phys. Rev. B* **76**, 235313 (2007); T. Meunier, I. T. Vink, L. H. Willems van Beveren, K.-J. Tielrooij, R. Hanson, F. H. L. Koppens, H. P. Tranitz, W. Wegscheider, L. P. Kouwenhoven, and L. M. K. Vandersypen, *Phys. Rev. Lett.* **98**, 126601 (2007); L. R. Schreiber, F. R. Braakman, T. Meunier, V. Calado, J. Danon, J. M. Taylor, W. Wegscheider, and L. M. K. Vandersypen, e-print arXiv:1010.5682v1.

¹⁸P. Stano and J. Fabian, *Phys. Rev. Lett.* **96**, 186602 (2006); V. N. Golovach, A. Khaetskii, and D. Loss, *Phys. Rev. B* **77**, 045328 (2008).

¹⁹C. Fasth, A. Fuhrer, L. Samuelson, V. N. Golovach, and D. Loss, *Phys. Rev. Lett.* **98**, 266801 (2007).

²⁰A. Pfund, I. Shorubalko, K. Ensslin, and R. Leturcq, *Phys. Rev. B* **76**, 161308(R) (2007).

²¹S. Takahashi, R. S. Deacon, K. Yoshida, A. Oiwa, K. Shibata, K. Hirakawa, Y. Tokura, and S. Tarucha, *Phys. Rev. Lett.* **104**, 246801 (2010).

²²V. I. Fal’ko, B. L. Altshuler, and O. Tsyplatyev, *Phys. Rev. Lett.* **95**, 076603 (2005); J. Könnemann, R. J. Haug, D. K. Maude, V. I. Fal’ko, and B. L. Altshuler, *ibid.* **94**, 226404 (2005).

²³M. Valiyn-Rodriguez, A. Puente, and Ll. Serra, *Eur. Phys. J. B* **39**, 87 (2004).

- ²⁴The in-plane electric field, F_y , originating from the potential difference between the source-drain electrodes in Ref. 21, is of order of hundreds of V cm^{-1} , which is 50 times smaller than the electric field in the growth direction. The effect of F_y on the energy levels was found to be negligible.
- ²⁵M. Stopa and C. M. Marcus, *Nano Lett.* **8**, 1778 (2008).
- ²⁶The accuracy of the two-electron calculation for an infinite-quantum-well-confinement potential has been checked by comparing the present calculation in the two-dimensional limit (in the z direction we use an infinite quantum well with width of 1 nm) with the two-dimensional calculation on the grid showing an accuracy better than $1 \mu\text{eV}$ with ground state energy $E = 3.574 \text{ meV}$. For parabolic confinement we compared the present computational scheme with the center-of-mass approach obtaining differences in the energy of order of tenth of μeV with the ground-state energy $E = 248.15 \text{ meV}$.
- ²⁷P. W. Fry *et al.*, *Phys. Rev. Lett.* **84**, 733 (2000).
- ²⁸See supplemental online material for S. Takahashi, R. S. Deacon, K. Yoshida, A. Oiwa, K. Shibata, K. Hirakawa, Y. Tokura, and S. Tarucha, *Phys. Rev. Lett.* **104**, 246801 (2010).
- ²⁹Evaluated from gate voltage $V_g = -0.8 \text{ V}$ for which the first current peak in tunneling spectroscopy is observed [see Ref. 28].
- ³⁰E. A. de Andrada e Silva, G. C. La Rocca, and F. Bassani, *Phys. Rev. B* **55**, 16293 (1997).
- ³¹W. Knap *et al.*, *Phys. Rev. B* **53**, 3912 (1996).
- ³²M. Willatzen and L. C. Lew Yan Voon, *J. Phys. Condens. Matter* **20**, 345216 (2008).
- ³³The energetic contribution to the AC calculated for $R_z = 10 \text{ nm}$ from the second and third term in Eq. (14) is 4 and $9 \mu\text{eV}$, respectively, and does not change when the dot height is increased to $R_z = 40 \text{ nm}$.
- ³⁴M. P. Nowak and B. Szafran, *Phys. Rev. B* **83**, 035315 (2011).
- ³⁵S. Prabhakar, J. E. Raynolds, and R. Melnik, e-print arXiv:1011.1921v1.
- ³⁶In a sufficiently strong magnetic field, the diamagnetic term of the Hamiltonian becomes stronger than the confinement potential and, in consequence, the Hamiltonian eigenstates become identical to Fock-Darwin states. In particular, the ground-state and the first excited state acquire angular momenta 0 and -1 , respectively. However, in the problem studied in this paper, including strong confinement in the growth direction and in plane magnetic field orientation, this limit is not reached within the considered range of B . Namely, for quantum dot with dimensions $R_x = 100 \text{ nm}$, $R_y = 60 \text{ nm}$ and $R_z = 10 \text{ nm}$ in the absence of SO coupling at $B = 10 \text{ T}$ we obtain mean values of the angular momentum 0.1, 0.1, 0.1, and 0.09 for the ground and three lowest energy excited states, respectively. For the dot with increased height, $R_z = 40 \text{ nm}$, the values are 0.8, 0.7, 0.6, and 0.4.